

University of Groningen

Bending of a single crystal

Yefimov, S.; Giessen, E. van der; Groma, I.; Groma, [No Value]

Published in:
Modelling and Simulation in Materials Science and Engineering

DOI:
[10.1088/0965-0393/12/6/002](https://doi.org/10.1088/0965-0393/12/6/002)

IMPORTANT NOTE: You are advised to consult the publisher's version (publisher's PDF) if you wish to cite from it. Please check the document version below.

Document Version
Publisher's PDF, also known as Version of record

Publication date:
2004

[Link to publication in University of Groningen/UMCG research database](#)

Citation for published version (APA):

Yefimov, S., Giessen, E. V. D., Groma, I., & Groma, N. V. (2004). Bending of a single crystal: discrete dislocation and nonlocal crystal plasticity simulations. *Modelling and Simulation in Materials Science and Engineering*, 12(6), 1069 - 1086. [PII S0965-0393(04)78192-9]. <https://doi.org/10.1088/0965-0393/12/6/002>

Copyright

Other than for strictly personal use, it is not permitted to download or to forward/distribute the text or part of it without the consent of the author(s) and/or copyright holder(s), unless the work is under an open content license (like Creative Commons).

The publication may also be distributed here under the terms of Article 25fa of the Dutch Copyright Act, indicated by the "Taverne" license. More information can be found on the University of Groningen website: <https://www.rug.nl/library/open-access/self-archiving-pure/taverne-amendment>.

Take-down policy

If you believe that this document breaches copyright please contact us providing details, and we will remove access to the work immediately and investigate your claim.

Downloaded from the University of Groningen/UMCG research database (Pure): <http://www.rug.nl/research/portal>. For technical reasons the number of authors shown on this cover page is limited to 10 maximum.

Bending of a single crystal: discrete dislocation and nonlocal crystal plasticity simulations

S Yefimov¹, E Van der Giessen^{1,3} and I Groma²

¹ Department of Applied Physics, Netherlands Institute for Metals Research, University of Groningen, Nijenborgh 4, 9747 AG Groningen, The Netherlands

² Department of General Physics, Eötvös University, Pazmany P. setany 1/a, Pf. 32 H-1518 Budapest, Hungary

E-mail: Giessen@phys.rug.nl

Received 25 November 2003


Published 31 August 2004

Online at stacks.iop.org/MSMSE/12/1069

doi:10.1088/0965-0393/12/6/002

Abstract

We have recently proposed a nonlocal continuum crystal plasticity theory that is based on a statistical-mechanics description of the collective behaviour of dislocations. Kinetic equations for the dislocation density fields have been derived from the equation of motion of individual dislocations and have been coupled to a continuum description of single slip. Dislocation nucleation, the material resistance to dislocation glide and dislocation annihilation are included in the formulation. The theory is applied, in this paper, to the problem of bending of a single-crystal strip in plane strain, using parameter values obtained previously from fitting to discrete dislocation results of a different boundary value problem. A numerical solution of the problem is obtained using a finite element method. The bending moment versus rotation angle and the evolution of the dislocation structure are analysed for different orientations and specimen sizes with due consideration of the role of geometrically necessary dislocations. The results are compared to those of discrete dislocation simulations of the same problem. Without any additional fitting of the parameters, the continuum theory is able to describe the dependence on slip plane orientation and on specimen size.

 This article features online multimedia enhancements

1. Introduction

Nonlocal or strain gradient continuum plasticity theories are extensions of classical (local) continuum descriptions that attempt to incorporate the size dependence of dislocation plasticity at length scales of around 1 μm , e.g. Hutchinson (2000). The development of such theories is

³ Author to whom any correspondence should be addressed.

a very active field currently, with a variety of theories which differ in the way nonlocality is incorporated. A subset of them is based on the idea that the geometrically necessary dislocations associated with strain gradients give rise to additional hardening. Most of these employ Nye's (1953) geometrical concept of the dislocation density tensor, but in a variety of ways. A central and still unresolved issue in the formulation of phenomenological strain gradient theories is whether additional boundary conditions are necessary, e.g. Aifantis (1984), Acharya and Bassani (2000), Bassani *et al* (2001), Gao and Huang (2003), Gurtin (2002), and Van der Giessen and Needleman (2003). Parallel to these developments there is work by, for instance, Arsenlis and Parks (2002) and Evers *et al* (2002) where a more direct physical connection is sought between dislocation density and hardening.

In a previous paper (Yefimov *et al* 2004) we have taken a somewhat different route by starting from a statistical description of the motion of an ensemble of parallel edge dislocations by Groma and co-workers (Groma 1997, Groma and Balogh 1999, Groma *et al* 2003). Averaging leads to two kinds of dislocation density for single slip: the standard total dislocation density and a dislocation–difference density that can be interpreted as the density of geometrically necessary dislocations. The analysis leads to two coupled transport equations for these densities, which form the nonlocal extension of a standard continuum slip model. It is these kinetic equations that introduces extra boundary conditions, and they directly relate to the flux of dislocations across boundaries. To assess the validity of the approach, we have applied it to the analysis of shearing of a model composite material in single slip, where impenetrable interfaces with the elastic reinforcing particles impose zero-flux boundary conditions. The free parameters in the theory have been fitted to results of (inherently nonlocal) discrete dislocation simulations of the same problem (Cleveringa *et al* 1997). It was shown that several key features of the discrete dislocation results, such as the dependence on particle shape and size, were correctly picked up by the nonlocal continuum theory (Yefimov *et al* 2004).

A necessary condition for a constitutive model to have predictive power is that, once fitted to a particular boundary value problem, it is able to predict other boundary value problems for the same material. The object of this paper is to perform this test for the model of Yefimov *et al* (2004) by applying it to bending, again in single slip. The key in this problem is that dislocations are completely free to leave the material, as opposed to the zero-flux conditions in the aforementioned shear problem. This paper will show how these boundary conditions can be represented in the present theory and will discuss the correspondence with results from discrete dislocation simulations.

2. Problem formulation

We consider the elastoplastic bending of a single crystal in single slip, as sketched in figure 1. A plane strain strip with width L and height h is subjected to a prescribed rotation along its edges. With the x_1 – x_2 plane being the plane of deformation, the imposed rotation θ is prescribed through the macroscopic boundary conditions

$$u_1(t) = \pm\theta x_2, \quad \sigma_{12} = 0 \quad \text{on } x_1 = \pm\frac{L}{2} \quad (1)$$

for the displacements u_i and σ_{ij} . Traction-free boundary conditions are imposed along the top and bottom of the strip:

$$\sigma_{12} = 0, \quad \sigma_{22} = 0 \quad \text{at } x_2 = \pm\frac{h}{2}. \quad (2)$$

The slip system is defined by the slip plane normal \mathbf{m} and the slip direction unit vector $\mathbf{s} = \mathbf{b}/|\mathbf{b}|$, where \mathbf{b} is the Burgers vector. The slip system orientation with respect to the x_1 direction is

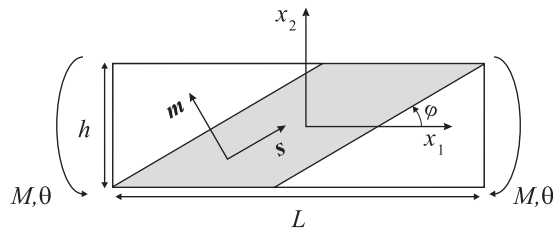


Figure 1. Sketch of the bending of a two-dimensional strip. Plastic deformation is allowed to take place in the hatched region only.

specified by the angle φ . Slip is permitted only within the hatched area of the strip indicated in figure 1 such that the lateral sides, where displacements are prescribed, always remain elastic.

No dislocations are presumed present initially and obstacles are not taken into account in the analysis. New dislocations are generated from Frank–Read sources distributed in the material. A constant macroscopic rotation rate, $\dot{\theta}$, is imposed until a specified rotation angle is reached. Then, the strip is unloaded by applying $\dot{\theta}$ in the opposite direction until θ reaches a value of zero. The effect of specimen size is studied by varying L and h such that the ratio h/L remains unchanged. The overall response will be presented in terms of the work-conjugate bending moment M , given by

$$M = \int_{-h/2}^{h/2} x_2 \sigma_{11} \left(\pm \frac{L}{2}, x_2 \right) dx_2 \quad (3)$$

and the applied rotation angle θ . The calculations are carried out within the context of small displacement gradients.

2.1. Discrete dislocation plasticity

A discrete dislocation plasticity analysis of the problem follows the formulation by Van der Giessen and Needleman (1995) and the application to bending by Cleveringa *et al* (1997). In this section we give a brief summary of the methodology, confining ourselves to two-dimensional boundary value problems and single slip.

The dislocations are modelled as line defects in a linear elastic continuum. The computation of the deformation history is carried out in an incremental manner. Each time step involves three main computational stages: (i) determining the forces on the dislocations, i.e. the Peach–Koehler force; (ii) determining the rate of change of the dislocation structure, which involves the motion of dislocations, the generation of new dislocations, their mutual annihilation and their possible pinning at obstacles; (iii) determining the stress and strain state for the updated dislocation arrangement. The fields are written as the superposition of fields, denoted by $(\tilde{\cdot})$, as if the dislocations were in infinite space, and the complementary (or image) fields, denoted by $(\hat{\cdot})$, correct for the actual boundary conditions. Thus, for the displacements and stresses,

$$\mathbf{u} = \tilde{\mathbf{u}} + \hat{\mathbf{u}}, \quad \boldsymbol{\sigma} = \tilde{\boldsymbol{\sigma}} + \hat{\boldsymbol{\sigma}}. \quad (4)$$

The $(\tilde{\cdot})$ are singular at the dislocations and are known analytically. The boundary value problem for the image fields is regular and can be solved by, e.g. the finite element method.

In this plane strain analysis, only edge dislocations are considered which are restricted to glide on their slip planes. The glide component of the Peach–Koehler force F^i acting on the

i th dislocation is given by

$$F^i = \mathbf{m}^i \cdot \left(\hat{\boldsymbol{\sigma}} + \sum_{j \neq i} \boldsymbol{\sigma}^j \right) \cdot \mathbf{b}^i \quad (5)$$

and includes the interactions with all other dislocations in the material. The glide velocity v^i of the dislocation i along s^i is taken to be linearly related to the Peach–Koehler force through the drag relation

$$F^i = Bv^i \quad (6)$$

with drag coefficient B .

New dislocations are generated by mimicking the Frank–Read mechanism. In two dimensions, a Frank–Read source is emulated by a point source on the slip plane which generates a dislocation dipole when the magnitude of the resolved shear stress at the source exceeds the source strength τ_{nuc} during a period of time t_{nuc} . The distance L_{nuc} between the newly generated dislocations is specified as

$$L_{\text{nuc}} = \frac{\mu}{2\pi(1-\nu)} \frac{b}{\tau_{\text{nuc}}}. \quad (7)$$

where μ is the shear modulus and ν is Poisson's ratio. Annihilation of two dislocations on the same slip plane with opposite Burgers vectors occurs when they are within a material-dependent, critical annihilation distance, L_e .

2.2. Nonlocal continuum plasticity

The nonlocal continuum crystal plasticity formulation adopted here is based on the theory proposed by Yefimov *et al* (2004). The theory is developed for single slip and involves a statistical-mechanics description of the collective behaviour of dislocations coupled to the standard description of single crystal continuum slip.

In summary, the plastic part $\dot{\boldsymbol{\epsilon}}^p$ of the strain rate,

$$\dot{\boldsymbol{\epsilon}} = \dot{\boldsymbol{\epsilon}}^e + \dot{\boldsymbol{\epsilon}}^p \quad (8)$$

is expressed, as is usual in single slip, in terms of the slip rate ($\dot{\gamma}$) on the slip system, as

$$\dot{\boldsymbol{\epsilon}}^p = \frac{1}{2} \dot{\gamma} (\mathbf{s} \otimes \mathbf{m} + \mathbf{m} \otimes \mathbf{s}), \quad (9)$$

but with $\dot{\gamma}$ being linked to the average continuum dislocation glide velocity (v) given by

$$v = B^{-1} \mathbf{b} (\tau - \tau_s). \quad (10)$$

Here, as an approximation (see Yefimov *et al* (2004)), τ is the resolved shear stress,

$$\tau = \mathbf{m} \cdot \boldsymbol{\sigma} \cdot \mathbf{s} \quad (11)$$

and B is the same drag coefficient as in (6). To take into account the effect of obstacles on the slip plane in the form of small precipitates or forest dislocations, Yefimov *et al* (2004) introduced the additional (and completely phenomenological) notion that the response of the material is elastic, i.e. $\dot{\gamma} = 0$, when

$$|\tau - \tau_s| < \tau_{\text{res}}, \quad (12)$$

where τ_{res} is the slip resistance.

The back stress τ_s in equations (10) and (12) follows from the state variable field description in terms of the total dislocation density, ρ , and the net Burgers vector density, k , which is an

integral part of the theory. A statistical treatment of an ensemble of gliding dislocations by Groma (1997) leads to the following coupled balance equations:

$$\frac{\partial \rho}{\partial t} + \frac{\partial}{\partial \mathbf{r}} \cdot (k\mathbf{v}) = f(\rho, k, \dots), \quad (13)$$

$$\frac{\partial k}{\partial t} + \frac{\partial}{\partial \mathbf{r}} \cdot (\rho\mathbf{v}) = 0, \quad (14)$$

with the back stress arising from the gradient of the net Burgers vector density along the slip direction, according to

$$\tau_s(\mathbf{r}) = \frac{\mu \mathbf{b}}{2\pi(1-\nu)\rho(\mathbf{r})} \cdot D \frac{\partial k}{\partial \mathbf{r}}. \quad (15)$$

Here, D is a dimensionless constant on the order of unity (see Zaiser *et al* (2001)).

The function f in the right-hand side of equation (13) is the source term to the total dislocation density and is taken to have the form

$$f(\rho, k, \dots) = C\rho_{\text{nuc}}|\tau - \tau_s| - AL_e(\rho + k)(\rho - k)|\mathbf{v}|. \quad (16)$$

The first term in the right-hand side of equation (16) represents nucleation from sources with a density ρ_{nuc} and at a rate governed by the parameter C , given by

$$C = \frac{1}{\tau_{\text{nuc}}t_{\text{nuc}}} \quad \text{if } |\tau - \tau_s| \geq \tau_{\text{nuc}}; \quad C = 0 \quad \text{otherwise}, \quad (17)$$

in terms of the nucleation strength τ_{nuc} and the nucleation time t_{nuc} . The second term in the right-hand side describes the annihilation of dislocations at a rate determined by $A|\mathbf{v}|$, with A being a dimensionless constant. Details can be found in Yefimov *et al* (2004).

The constitutive model is supplemented with the elastic strain rate $\dot{\epsilon}^e$ being governed by Hooke's law in the form,

$$\dot{\epsilon}^e = \mathbf{L}^{-1} \dot{\boldsymbol{\sigma}} \quad (18)$$

with $\dot{\boldsymbol{\sigma}}$ the stress rate and \mathbf{L} the tensor of elastic moduli, which is expressed in terms of μ and ν for isotropic elasticity.

In addition to the macroscopic mechanical boundary conditions (1) and (2), 'microscopic' boundary conditions on the dislocation dynamics equations (13) and (14) are required. Taking into account that slip is confined to the plastic zone in figure 1 the kinetic boundary conditions are specified only along its boundary S . This boundary consists of the part $S_1 = \{x_2 = x_1 \tan \varphi \pm \frac{1}{2}(h - L \tan \varphi)\} \subset S$ along the elastic–plastic interfaces and $S_2 = S \setminus S_1$ at the top and bottom surfaces $\{x_2 = \pm h/2\}$. The S_1 boundary is parallel to the slip planes, so that in single slip

$$v_{\perp} = \mathbf{v} \cdot \mathbf{m} = 0 \quad \text{along } S_1. \quad (19)$$

If S_1 is not parallel to the slip planes, it may be physically reasonable to assume that this boundary is impenetrable for dislocations so that the normal flux $\mathbf{v} \cdot \mathbf{n} = 0$ with \mathbf{n} the normal to S_1 .

Along S_2 —the free surfaces—natural dislocation outflow occurs. Dislocation nucleation at the surfaces is not taken into account and therefore there is no additional dislocation inflow from the surfaces. There are several choices for a boundary condition when a flow is expected to go out of the computational domain, e.g. continuative, periodic, outflow, natural etc. Which would be the best depends on the physical conditions of the problem. Continuative boundary conditions comprise zero normal derivatives at the 'open' boundary and are intended to represent a smooth continuation of the flow through the boundary, and is used for example

in studies by Zienkiewicz *et al* (1985) and Peraire (1986). However, this type of boundary conditions has no strong physical basis, but rather is a mathematical statement which in some situations provides the desired flow behaviour. In this study, we assume that, as in the discrete dislocation simulations, dislocations leave the domain with no reflection from the surfaces and that there is no additional inflow. Thus, a physically meaningful boundary condition at S_2 is a natural boundary condition rather than an essential one. However, we do not explicitly impose the boundary condition on the continuous problem (equations (13) and (14)), but implicitly, within its approximation by the finite element method, as discussed in the following section. This approach is similar to the successful treatment by Papanastasiou *et al* (1992) of the outflow boundary in finite element simulations of the Navier–Stokes equations with no boundary condition at the outflow boundary.

2.2.1. Numerical implementation of the continuum model The dislocation density evolution equations (13) and (14) supplemented with the boundary conditions (19) represent a nonlinear convection-dominated diffusion problem coupled to the single crystal continuum plasticity model described in the above section. A standard finite element method is employed to solve this set of equations (see Yefimov *et al* (2004) for details).

The dislocation evolution part of the problem and the crystal plasticity part can be decoupled by applying a staggered solution procedure for time integration. The solution of either of the two separate problems is obtained by using an explicit time-stepping scheme, with the same time steps for both subproblems. In principle, we may adopt independent spatial discretizations for the two parts of the problem, but we take the two meshes to be identical for convenient passing of information. The spatial discretization uses quadrilateral elements consisting of four crossed linear triangular elements.

The solution of the crystal plasticity part departs directly from the incremental version of the principle of virtual work. The associated boundary conditions have already been listed in equations (1) and (2).

In addition, we solve the evolution equations (13) and (14) in the plastic zone using a standard weighted-residual Galerkin method. Generally, the Galerkin discretization is not applicable for solving convection-dominated diffusion problems due to oscillatory behaviour of the solution, unless element Peclet numbers are small enough. However, for the particular case of systems without a specification of boundary conditions at free surfaces, standard Galerkin weighting results in quite acceptable solutions even for quite high Peclet numbers (Zienkiewicz and Taylor 1991).

The spatial discretization is based on the interpolation of ρ and k , as well as their rates, inside an element from the nodal values; e.g. $\rho = N^T \boldsymbol{\rho}$, $k = N^T \mathbf{k}$, where $\boldsymbol{\rho}$ and \mathbf{k} are the vectors of nodal values of the dislocation densities ρ and k , respectively, and N is the vector of the C_0 continuous shape functions. As a consequence, the back stress according to equation (15),

$$\tau_s = b \frac{T}{\rho} \frac{\partial k}{\partial \mathbf{r}} \cdot \mathbf{s}, \quad T = D \frac{\mu}{2\pi(1-\nu)}, \quad (20)$$

is governed by lower-dimensional interpolation. Therefore, we take the back stresses to be defined at the integration points of elements, just like the resolved shear stress from equation (11).

After substitution of equation (20) and evaluation of the weighted residual integral for the balance law (14) for k , for instance, we obtain the system of linear equations

$$M\dot{\mathbf{k}} = J\boldsymbol{\rho} - H\mathbf{k} - \mathbf{f}. \quad (21)$$

Here, the matrices \mathbf{M} , \mathbf{J} and \mathbf{H} are given by

$$\mathbf{M} = \int_{-L/2}^{L/2} \int_{-h/2}^{h/2} \mathbf{N}\mathbf{N}^T dx_1 dx_2, \quad (22)$$

$$\mathbf{J} = B^{-1}b \int_{-L/2}^{L/2} \int_{-h/2}^{h/2} \tau \mathbf{N} \frac{\partial \mathbf{N}^T}{\partial \mathbf{r}} \cdot \mathbf{s} dx_1 dx_2 \quad (23)$$

and

$$\mathbf{H} = B^{-1}b^2 \int_{-L/2}^{L/2} \int_{-h/2}^{h/2} T \mathbf{s} \cdot \frac{\partial \mathbf{N}}{\partial \mathbf{r}} \frac{\partial \mathbf{N}^T}{\partial \mathbf{r}} \cdot \mathbf{s} dx_1 dx_2. \quad (24)$$

The right-hand side vector

$$\mathbf{f} = \int_{S_1} \mathbf{N}^T \rho \mathbf{v} \cdot \mathbf{n} ds + \int_{S_2} \mathbf{N}^T \rho \mathbf{v} \cdot \mathbf{n} ds = \int_{S_2} \mathbf{N}^T \rho \mathbf{v} \cdot \mathbf{n} ds \quad (25)$$

(s being a coordinate along the surface) contains contributions from the boundaries S_1 and S_2 . The contribution from S_1 in equation (25) vanishes due to the boundary condition (19) with $\mathbf{n} = \mathbf{m}$ on S_1 . The remaining S_2 contribution, through the natural boundary outflux condition, is just evaluated from the velocity field along S_2 that is computed using equation (10). The latter boundary condition is unusual because, in the weak formulation, it appears to impose no boundary condition at all on the dislocation densities outflow.

The spatial discretization of equation (13) is done in a manner fully similar to that for equation (14) and is not presented, for brevity.

3. Results

The nonlocal crystal plasticity model described in the previous section is applied to the problem of bending of a single crystal. The results are compared with those of discrete dislocation plasticity simulations of the problem. The discrete dislocation plasticity simulations are based on the work of Cleveringa *et al* (1999).

3.1. Reference case

The results for a strip of dimensions $L = 12 \mu\text{m}$ and $h = 4 \mu\text{m}$ subjected to a bending rate of $\dot{\theta} = 10^3 \text{ s}^{-1}$ will serve as a reference for subsequent parameter studies. The slip system is oriented at $\varphi = +30^\circ$ from the x_1 axis. The same material parameters have been used, whenever possible, as in the discrete dislocation calculations of Cleveringa *et al* (1999), both for elastic and dislocation properties. In contrast to Cleveringa *et al*, however, we do not incorporate obstacles in our analysis. The material is taken to be elastically isotropic, with shear modulus $\mu = 26.3 \text{ GPa}$ and Poisson ratio $\nu = 0.33$. The magnitude of the Burgers vector is $b = 0.25 \text{ nm}$ for all (edge) dislocations, and a value $B = 10^{-4} \text{ Pa s}$, for the drag coefficient, is taken.

A uniform finite element mesh consisting of 66×38 quadrilateral elements is used to discretize the domain for both mechanical and dislocation dynamics sub-problems. For the latter sub-problem we define a plastic subdomain bounded by S as discussed in the above. To treat the degrees of freedom at the elastic–plastic interfaces, S_1 , the mesh has been designed so that one of two diagonals of any element is parallel to S_1 . The interface can then be simply discretized by letting two of the four sub-triangles of a boundary quadrilateral fall inside the plastic domain and the other two in the elastic domain. Compatibility between the

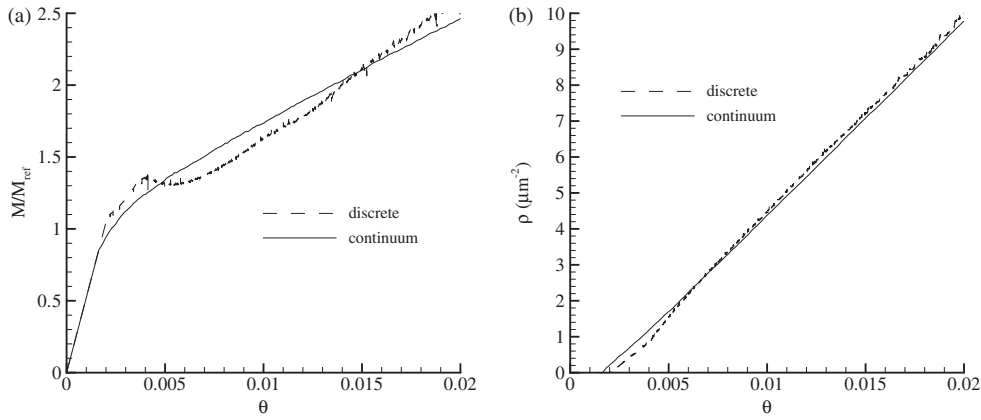


Figure 2. Comparison of (a) bending moment, M , versus imposed rotation, θ , curves and (b) evolution of the total dislocation density ρ , for the reference case according to nonlocal continuum and discrete dislocation plasticity.

subdomains at the interface S_1 is thus achieved without additional mesh refinement. The mesh size dependence of the solution will be discussed later in this section.

In the discrete dislocation calculations the active slip planes are distributed with a uniform spacing of $100b$ inside the plastic zone, so that none of them intersects the lateral sides $x_1 = \pm L/2$ where displacements are prescribed. The material is taken to be initially dislocation free, and two dislocation sources are randomly positioned on each slip plane. Thus, for the reference case, there are a total of 101 slip planes and 202 sources. This leads to an average source density $\rho_{\text{nuc}} = 10 \mu\text{m}^{-2}$ (inside the plastic zone) that enters the nonlocal continuum model as a material parameter. In both discrete and continuum approaches, the strength of the dislocation sources is chosen randomly from a Gaussian distribution with mean value $\bar{\tau}_{\text{nuc}} = 1.9 \times 10^{-3} \mu$ and standard deviation $\Delta\tau_{\text{nuc}} = 0.2\bar{\tau}_{\text{nuc}}$, the nucleation time is taken to be $t_{\text{nuc}} = 2.6 \times 10^6 B/\mu$ for all sources and $L_c = 6b$. In the nonlocal continuum calculations the sources are distributed uniformly over all integration points in the matrix, with a uniform density ρ_{nuc} .

The continuum theory has a few free parameters: the coefficient D in the back stress (15); the slip resistance τ_{res} (cf equation (12)); and the annihilation coefficient A . Their values do not follow from the derivation and were fitted by Yefimov *et al* (2004) to discrete dislocation simulations for the problem of shearing of a two-dimensional composite material. The same values, $A = 5$, $D = 1$ and $\tau_{\text{res}} = 15 \text{ MPa}$, are employed in this study. Hence, no further fitting is being done later in this paper.

The bending moment response to the imposed rotation according to both plasticity descriptions is shown in figure 2(a). The moment M is normalized by a reference moment, M_{ref} , defined as

$$M_{\text{ref}} = \frac{2}{h} \int_{-h/2}^{h/2} \bar{\tau}_{\text{nuc}} x_2^2 dx_2 = \frac{2}{3} \bar{\tau}_{\text{nuc}} \left(\frac{h}{2} \right)^2. \quad (26)$$

This reference moment is the moment that would result from the linear stress distribution over the height: $\bar{\tau}_{\text{nuc}} x_2 / (h/2)$.

The initiation of plasticity is caused by the motion of the first generated dislocations and depends quite strongly on the position of the weakest sources relative to the outer fibres of the strip. These results suggest that the initial yield point is a stochastic quantity to a certain

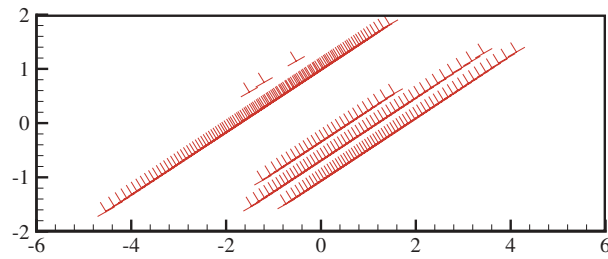


Figure 3. Dislocation distribution at $\theta = 0.015$ for the reference case. The corresponding movie can be found at stacks.iop.org/MSMSE/12/1077

(This figure is in colour only in the electronic version)

extent, and this effect is more pronounced in the discrete dislocation calculations due to the natural discreteness of the dislocation events. The ultimate hardening in the bending-moment-rotation curves, however, is hardly affected by the source distribution and controlled largely by the average source strength. The two models predict similar behaviour of the material with an almost linear increase of bending moment with rotation. The prediction of the continuum model for the total dislocation density evolution is also in good agreement with the discrete dislocation simulations, figure 2(b).

The discrete dislocation distribution at $\theta = 0.015$ is shown in figure 3. Only a few of the 101 available slip planes have been activated, and those are now heavily populated with dislocations. The dislocations are arranged in well-defined long pile-ups with dislocation-free areas near the free surfaces (because of the attraction by the surfaces). Only dislocations of the same sign are present in the material; the ones with the opposite sign have exited the material through one of the free surfaces. Thus, the dislocation density is the minimum required density to accommodate the applied deformation by producing local rotations; all dislocations at this stage are 'geometrically necessary'.

The continuum dislocation distributions at $\theta = 0.015$ are shown in figures 4(a) and (b) in terms of the ρ and k fields, respectively. Qualitatively, these fields show similar dislocation structures to those found in the discrete dislocation analysis of figure 3. The levels of the total dislocation density, ρ , and the net Burgers vector density, k , are practically identical, implying that positive dislocations dominate in the material and that they are all geometrically necessary, as in the discrete simulations. We also see (especially from the enhanced moving version of the figure) that the dislocations form pile-ups, which originate near the free surfaces and accumulate towards the centre of the strip. The continuum model predicts dislocation-free boundary layers near the free surfaces, much like the discrete simulations. However, near a neutral line at $x_2 = 0$, where the applied resolved shear stress τ vanishes, the continuum model shows a different dislocation structure than that from the discrete dislocations simulations. Due to a zero contribution of τ to the total driving stress, the dislocations are driven only by self-produced back stress τ_s . The discrete dislocation results, as figure 3 shows, reveal a dislocation flow through the neutral line even in the absence of τ , while in the continuum simulations, a narrow dislocation free zone occurs. This zone appears due to the applied slip resistance $\tau_{\text{res}} = 15$ MPa in the threshold condition (12). The width of the zone is controlled by the value of the slip resistance. Figure 5 shows the distribution of the total dislocation density in case of no slip resistance. These results reveal no dislocation free zone near the neutral line $x_2 = 0$, and are qualitatively similar to those from the discrete dislocation simulations.

Figure 6 demonstrates how the strip bends by showing the deformed finite element mesh. The deformation pattern is characterized by bands of localized deformation in the slip direction

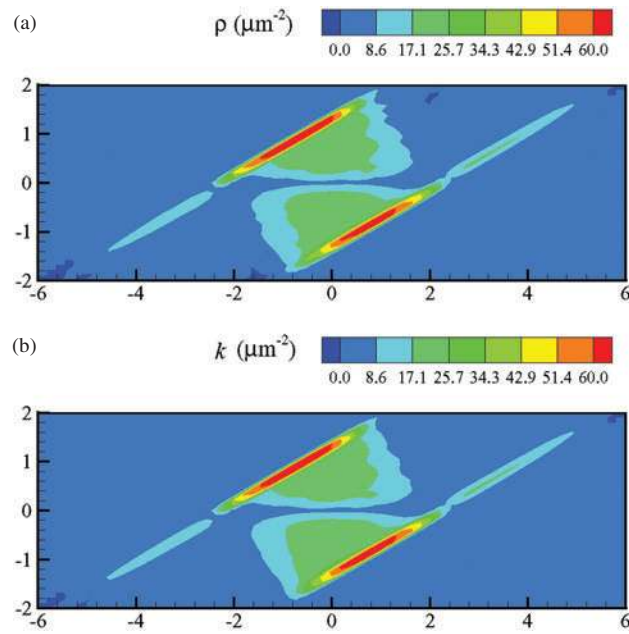


Figure 4. Distributions of (a) the total dislocation density ρ and (b) the sign-dislocation density k at $\theta = 0.015$ for the reference case. The corresponding movie for the density ρ can be found at stacks.iop.org/MSMSE/12/1078

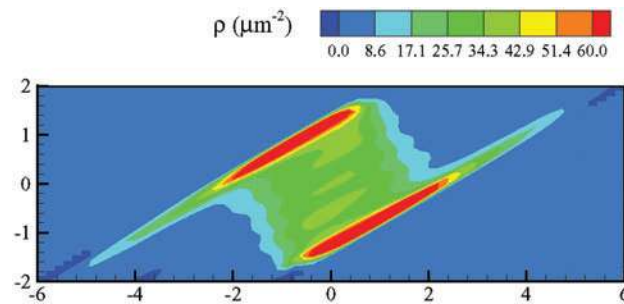


Figure 5. Distribution of the total dislocation density ρ at $\theta = 0.015$ for the reference case with $\tau_{\text{res}} = 0$.

and by slip steps at the free surfaces created by dislocations exiting the material. The continuum deformation pattern (figure 6(b)) is evidently smoother since localized flow now has to be represented through the finite elements. In the discrete dislocation computations localization comes from the displacement discontinuities across the slip planes, which are represented analytically (cf Cleveringa *et al* (1999)).

The respective distributions of σ_{11} are shown in figure 7. In both types of calculation, the material is relaxed near the free surfaces due to the outflow of negative dislocations and more stressed close to the faces of the elastic–plastic interface inside the strip. The latter feature gives rise to the continued dislocation generation activity seen in figures 3 and 4. The continuum prediction (figure 7(b)) obviously does not exhibit the stress fluctuations seen in the discrete dislocation field (figure 7(a)), because these are due to the individual dislocation singularities.

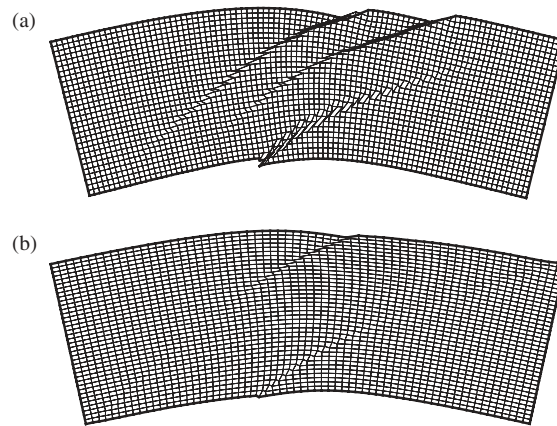


Figure 6. Deformed finite element mesh for the reference case at $\theta = 0.015$. (a) Discrete dislocation plasticity. (b) Nonlocal continuum plasticity. Displacements are multiplied by 20.

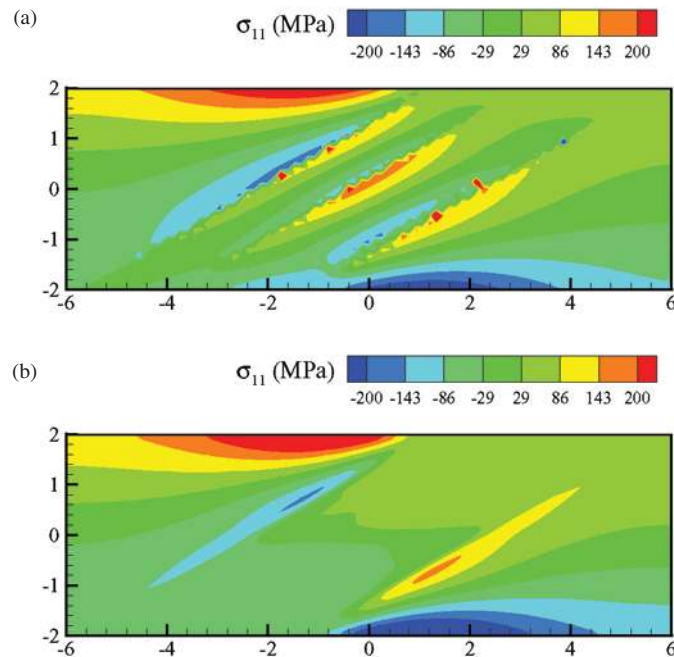


Figure 7. Distribution of σ_{11} for the reference case at $\theta = 0.015$. (a) Discrete dislocation plasticity. (b) Nonlocal continuum plasticity.

The behaviour of the material upon unloading is shown in figure 8. The discrete dislocation results reveal a distinct Bauschinger effect, but this is much less so for the continuum model. To study the possible reasons for such a significant qualitative difference, a simulation with zero slip resistance, $\tau_{\text{res}} = 0$, instead of the reference value $\tau_{\text{res}} = 15$ MPa, has been performed. Comparison of the results for these two values of τ_{res} reveals that the dislocations, which were not participating in plastic flow due to the threshold condition (12) in the reference case, contribute significantly to the overall response. The effect of no slip resistance leads to a

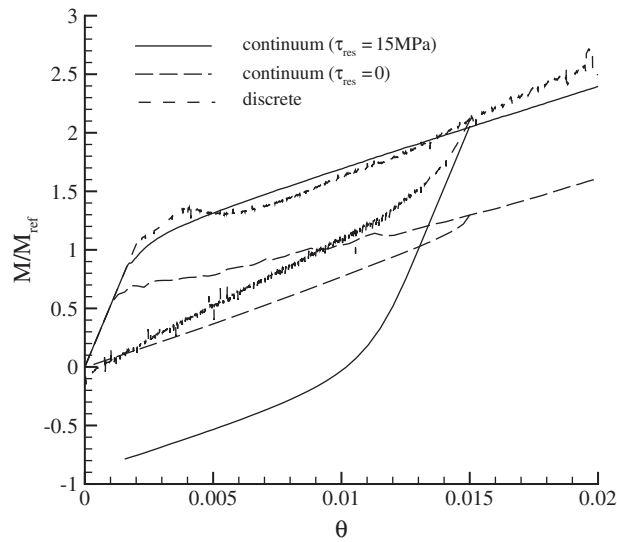


Figure 8. Comparison of moment–rotation curve for forward bending loading and unloading from $\theta = 0.015$ according to nonlocal continuum and discrete dislocation plasticity. Nonlocal plasticity results with $\tau_{\text{res}} = 0$ instead of 15 MPa are shown for comparison.

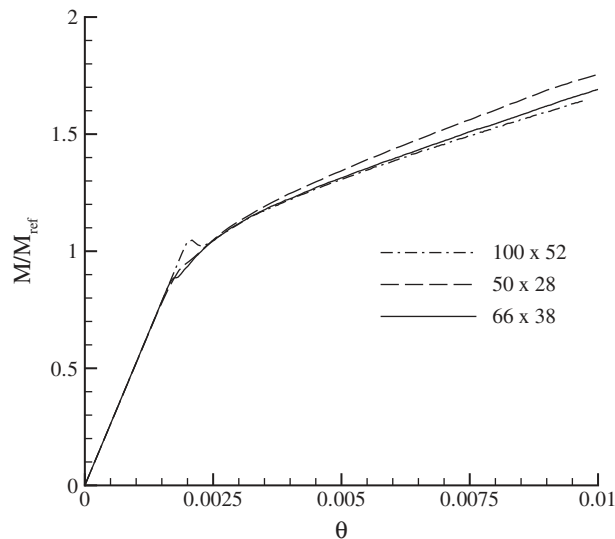


Figure 9. Moment versus rotation angle for the reference case using three finite element discretizations.

significant drop of the yield point, but the ultimate hardening rate remains unchanged. Upon unloading the Bauschinger effect that leads to nearly zero residual plastic deformation and seen in the discrete dislocation calculations, is picked up.

To analyse the mesh size dependence of the numerical solution of the continuum problem, a sequence of calculations with different mesh sizes was performed. A comparison of the results in terms of bending moment versus rotation angle curves is shown in figure 9. The coarser

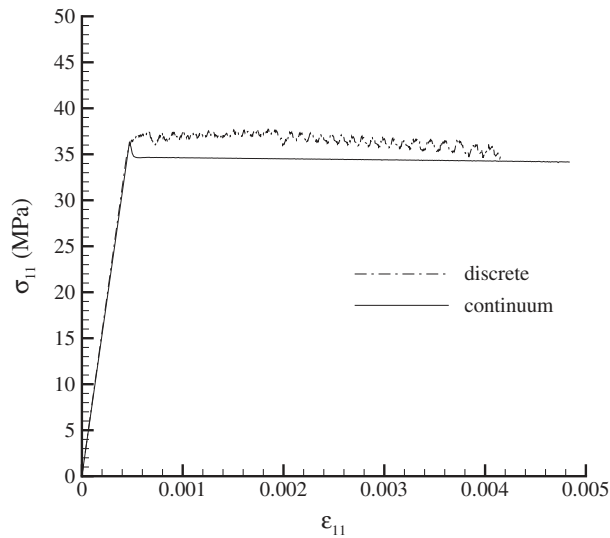


Figure 10. Comparison of σ - ϵ curves in plane strain tension for the reference case according to nonlocal continuum and discrete dislocation plasticity.

50×28 mesh gives a somewhat higher moment with respect to the reference 66×38 and finer 100×58 meshes. A significant difference between the finer meshes and the reference ones is seen only at the initial stage of plastic deformation. It is due to a difference in spatial distribution of the nucleation strength of sources, which is dependent upon a number of integration points of the mesh. For larger strains, the curves for the reference mesh and the finer one almost coincide. From this comparison, we conclude the reference mesh to be sufficiently fine to produce nearly mesh-size independent results, consuming less computation power than is necessary for the finer mesh.

Bending necessarily involves a strain gradient. For comparison, a tensile test calculation was performed for the same strip using both plasticity models. Figure 10 shows the calculated stress response to plane strain tension in the x_1 -direction. The boundary conditions are stress-free surfaces at $x_2 = \pm h/2$ as in the bending test, and a prescribed uniform fixed displacement rate \dot{u}_1 at $x_1 = \pm L/2$. As seen in figure 10, the two models predict that the material exhibits essentially perfect plasticity. The wiggles in the discrete dislocation curve are due to the discrete nucleation events. The deformed mesh in figure 11 shows that the plastic deformation is highly localized within one slip band. The discrete dislocation and continuum plasticity calculations predict different locations of the slip band (see figures 11(a) and (b)). This arises from different source distributions and therefore from different locations of the weak sources in those calculations. This is also responsible for the difference in yield stress seen in figure 10.

3.2. Effect of slip orientation

The ability of the continuum theory to pick up the effect of different slip orientations is studied by repeating the calculation for a slip plane orientation of $\varphi = 60^\circ$. Figure 12(a) shows the bending moment response according to the two models, in comparison with the $\varphi = 30^\circ$ reference case. In both cases the material exhibits nearly linear hardening, but for the case of 60° the tangent modulus is somewhat lower than that for the 30° case.

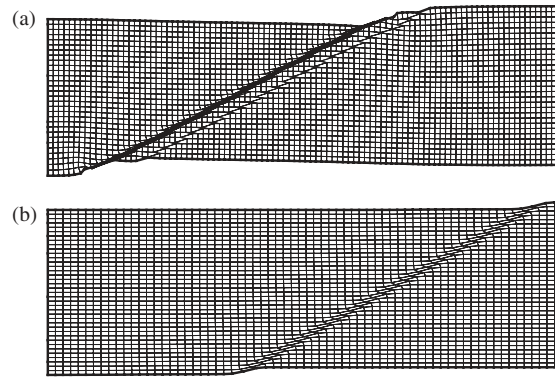


Figure 11. Deformed finite element mesh for the reference case in plane strain tension at $\epsilon = 0.0035$. (a) Discrete dislocation plasticity. (b) Nonlocal continuum plasticity. Displacements are multiplied by 20.

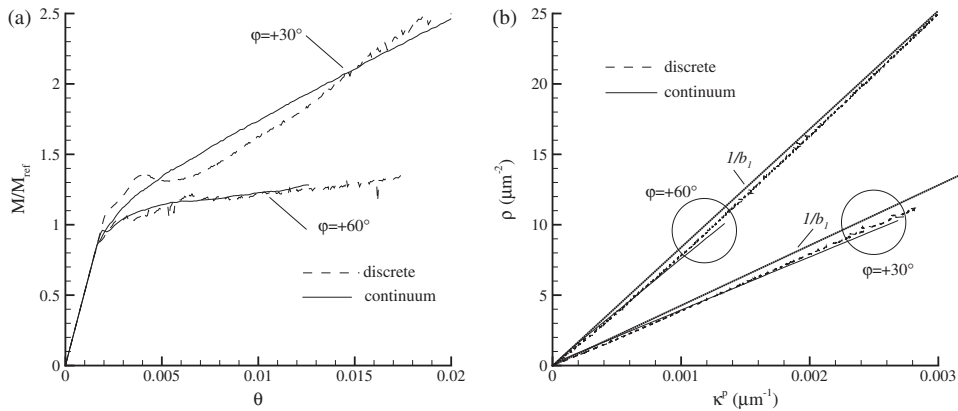


Figure 12. The effect of slip plane orientation on (a) the moment versus rotation curve and (b) the evolution of the total dislocation density versus plastic curvature.

According to figure 12(b), the total dislocation density increases linearly with the plastic curvature κ^p for both slip orientations. The plastic curvature is computed at each deformation stage as

$$\kappa^p = \frac{2\theta}{L} - \frac{M}{EI} \quad (27)$$

(cf Cleveringa *et al* (1999)). The first term in the right-hand side is the total curvature and the second is the elastic curvature, where $EI = \mu h^3/6(1 - \nu)$ is the bending stiffness in plane strain. According to Nye (1953) and Ashby (1970), the GND density for bending is

$$\rho_G = \frac{\kappa^p}{b_1}, \quad (28)$$

where $b_1 = b \cos \varphi$ is the component of the Burgers vector parallel to the x_1 -axis. This relation implies that the GND density increases linearly with the curvature κ^p . This line is plotted in figure 12(b) for comparison, from which we see that the simulations predict the dislocation density to grow with a slope slightly smaller than $1/b_1$. This deviation has been

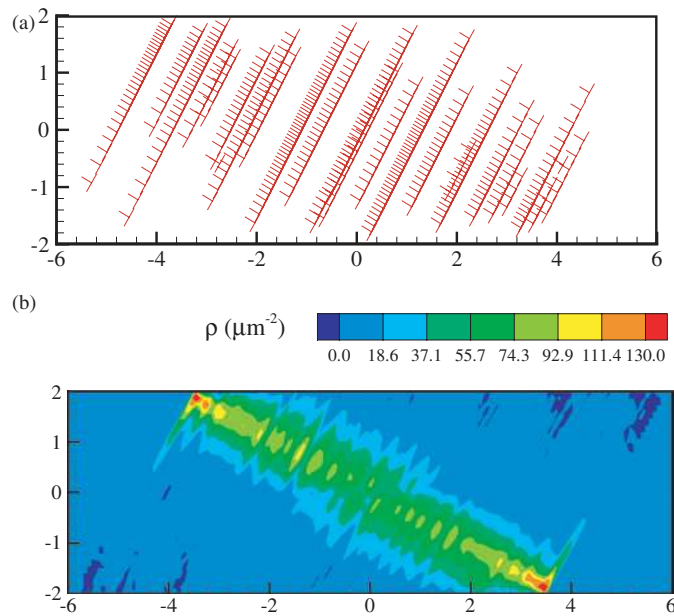


Figure 13. Distribution of (a) dislocations according to discrete dislocation plasticity and (b) the total dislocation density ρ at $\theta = 0.015$. The corresponding movies can be found at stacks.iop.org/MSMSE/12/1083

explained by Cleveringa *et al* (1999) to arise from the dislocation-free layers near the free surfaces (see figures 3, 4 and 13).

Figure 13 shows that, as b_1 is smaller, there are indeed many more dislocations in the 60° specimen than in the reference case (see figures 3 and 4), where only few slip planes are activated near the elastic–plastic interface. Also, the dislocation distribution inside the plastic zone is more uniform in comparison to the reference case. The continuum model (figure 13(b)) is able to resolve to some extent the formation of individual slip bands seen in the discrete dislocation simulations (figure 13(a)).

3.3. Size effects

Next we consider the effect of specimen size on the bending response of the strip. Figure 14(a) compares the response for the reference $12\ \mu\text{m} \times 4\ \mu\text{m}$ specimen with that of a two times smaller specimen ($6\ \mu\text{m} \times 2\ \mu\text{m}$) for one slip system at $+30^\circ$. Both specimens have the same source density as defined in the reference case. For the discrete dislocation simulations, random distributions of position and strength of the sources are generated independently for the two specimens, so that this by itself can give some statistical difference in the response in addition to the size effect. The continuum plasticity calculations use the same Gaussian distribution of source strength as generated for the reference case. Due to the presence of the GNDs, the specimen exhibits a size-dependent bending response, consistent with the conventional tendency of ‘smaller being stronger’ at this size scale. This size effect is not only predicted by discrete dislocation plasticity (Cleveringa *et al* 1999), but also by the continuum strain gradient theory used here. The size effect for crystals with a slip system at $+60^\circ$ is shown in figure 14(b).

Figures 14(a) and (b) also reveal that the size effect is mainly associated with the hardening rate increasing with decreasing specimen size. The overall hardening for all sizes and slip

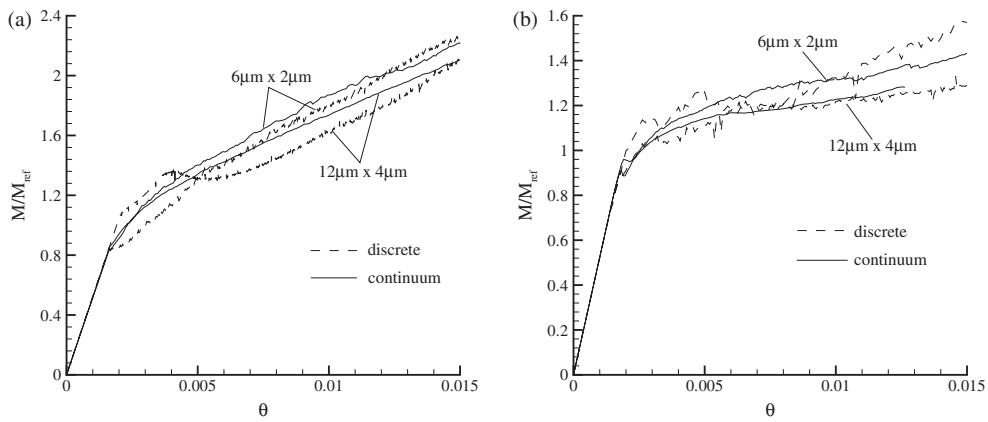


Figure 14. Effect of specimen size for slip systems at (a) $+30^\circ$ or (b) $+60^\circ$ on the moment versus rotation angle according to nonlocal continuum and discrete dislocation plasticity.

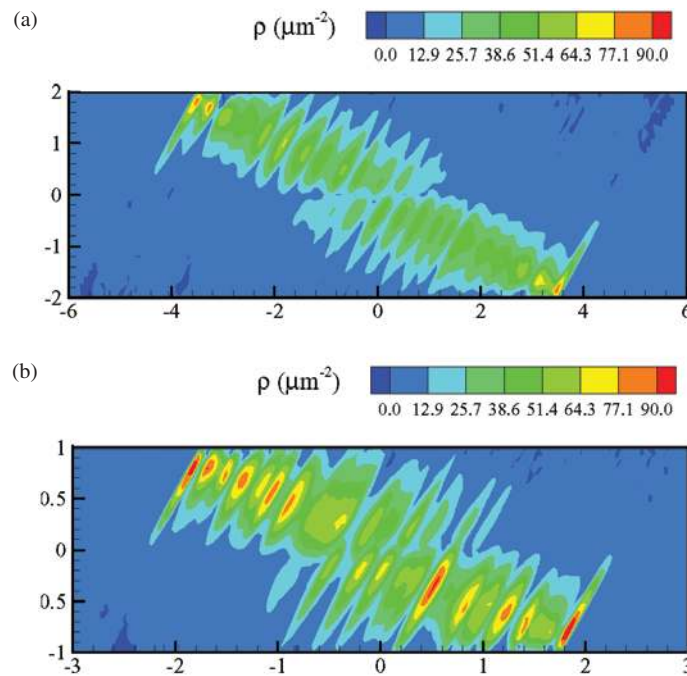


Figure 15. Distributions of the total dislocation density ρ for the cases in figure 13 at $\theta = 0.01$. (a) $12\ \mu\text{m} \times 4\ \mu\text{m}$; (b) $6\ \mu\text{m} \times 2\ \mu\text{m}$.

orientations appears to be approximately linear with rotation. A size effect on the yield point found in discrete dislocation simulations is only owing to different probabilities of finding a weak source near the highly stressed outer fibres.

Figure 15 compares the total dislocation density distributions for two different specimen sizes for $\varphi = 60^\circ$ at the same rotation. One observes that the number of pronounced slip bands is nearly the same for the two specimens, so that the mean spacing between the slip

bands scales linearly with the specimen size. This feature has been observed earlier in the discrete dislocation plasticity study by Cleveringa *et al* (1999). There it has been explained as a consequence of the competition between dislocations in a pile-up being geometrically necessary and repelling each other. Apparently, the continuum theory is able to pick these effects up as well.

4. Conclusion

We have applied the recently formulated nonlocal crystal plasticity theory (Yefimov *et al* 2004) to the bending of a single crystal by single slip. This boundary-value problem involves a number of free boundaries and we have discussed the treatment of the boundary conditions for the dislocation transport equations. It turns out that free outflux of dislocations across such boundaries is automatically captured by natural boundary conditions where the flux is just computed from the average dislocation equation of motion. This contrasts the zero-flux boundary conditions adopted in the composite shear problem considered previously (Yefimov *et al* 2004).

The continuum theory has a number of material parameters, most of which are analogous to parameters in the discrete dislocation model. It has an additional few ones that have been fitted by Yefimov *et al* (2004) to discrete dislocation dynamics simulations of the above-mentioned composite shear problem. Using these values, the bending response and the dislocation density distributions are outcomes of the continuum theory calculations. Compared with discrete dislocation dynamics results of the same problem, the continuum theory has proved to be capable of picking up: (i) the moment–rotation response; (ii) its size dependence; (iii) its dependence on slip plane orientation, as well as (iv) characteristics of the dislocation distributions.

This study together with the previous one (Yefimov *et al* 2004) belongs to a series of comparisons between nonlocal continuum theories and discrete dislocation simulations (e.g. Bassani *et al* (2001), Bittencourt *et al* (2002), Shu *et al* (2001)). The purpose of these works is to help the development of nonlocal theories (cf Van der Giessen and Needleman (2003)). Geometrically necessary dislocations play a central role in such theories, but their effects are implemented in quite different ways in the theories available at the moment. The present one is designed to be close to the dynamics of dislocations, which makes the form of the constitutive equations different from the ones considered in (Bassani *et al* 2001, Bittencourt *et al* 2002, Shu *et al* 2001). While the latter ones explicitly introduce a length scale as a material constant, the length scale in the present statistical-mechanics based theory enters implicitly through the source density ρ_{nuc} . Because of the physical origin of the dislocation evolution equations, the boundary conditions in the present theory are directly related, if not identical, to those in discrete dislocation theory, which make them physically transparent. A limitation of the current theory evidently is that it has been derived only for single slip. Zaiser *et al* (2001) have very recently made the first steps towards the extension to multiple slip.

In addition to this limitations, the theory currently suffers from the fact that it is two dimensional, as are the discrete dislocation simulations that were used for comparison. Three-dimensional discrete dislocation frameworks that account for aspects like junction formation and line tension are available these days (e.g. Kubin *et al* (1992), Weygand *et al* (2002)), but the statistical continuum theory needs to be developed. It is emphasized that this does not put a restriction on the conclusions of this paper. Not only is bending a two-dimensional problem when the crystal is properly oriented, the object here was to demonstrate that the continuum formulation is appropriate for traction-free boundary value problems, just as bending.

Acknowledgments

This research was carried out under project number MS97006 in the framework of the Strategic Research Programme of the Netherlands Institute for Metals Research in the Netherlands (www.nimr.nl). IG is grateful for support by the OTKA programme of the Hungarian Academy of Sciences under contract number T 030791.

References

- Acharya A and Bassani J L 2000 Incompatibility and crystal plasticity *J. Mech. Phys. Solids* **48** 1565–95
- Aifantis E C 1984 On the microstructural origin of certain inelastic models *J. Eng. Mater. Technol.* **106** 326–30
- Arsenlis A and Parks D M 2002 Modeling the evolution of crystallographic dislocation density in crystal plasticity *J. Mech. Phys. Solids* **50** 1979–2009
- Ashby M F 1970 The deformation of plastically non-homogeneous materials *Phil. Mag.* **21** 399
- Bassani J L, Needleman A and Van der Giessen E 2001 Plastic flow in a composite: a comparison of nonlocal continuum and discrete dislocation predictions *Int. J. Solids Struct.* **38** 833–53
- Bittencourt E, Needleman A, Gurtin M E and Van der Giessen E 2003 A comparison of nonlocal continuum and discrete dislocation plasticity predictions *J. Mech. Phys. Solids* **51** 281–310
- Cleveringa H H M, Van der Giessen E and Needleman A 1997 Comparison of discrete dislocation and continuum plasticity predictions for a composite material *Acta Mater.* **45** 3163–79
- Cleveringa H H M, Van der Giessen E and Needleman A 1999 A discrete dislocation analysis of bending *Int. J. Plast.* **15** 837–68
- Evers L P, Parks D M, Brekelmans W A M and Geers M G D 2002 Crystal plasticity model with enhanced hardening by geometrically necessary dislocation accumulation *J. Mech. Phys. Solids* **50** 2403–24
- Gao H and Huang Y 2003 Geometrically necessary dislocation and size-dependent plasticity *Scr. Mater.* **48** 113–18
- Groma I 1997 Link between the microscopic and mesoscopic length-scale description of the collective behaviour of dislocations *Phys. Rev. B* **56** 5807–13
- Groma I and Balogh P 1999 Investigation of dislocation pattern formation in a two-dimensional self-consistent field approximation *Acta Mater.* **47** 3647–53
- Groma I, Csikor F and Zaiser M 2003 Spatial correlations and higher-order gradient terms in a continuum description of dislocation dynamics *Acta Mater.* **51** 1271–81
- Gurtin M E 2002 A gradient theory of single-crystal viscoplasticity that accounts for geometrically necessary dislocations *J. Mech. Phys. Solids* **50** 5–32
- Hutchinson J W 2000 Plasticity at the micron scale *Int. J. Solids Struct.* **37** 225–38
- Kubin L P, Canova G, Condat M, Devincere B, Pontikis V and Bréchet Y 1992 *Solid State Phenomena* **23–24** 455–72
- Nye J F 1953 Some geometrical relations in dislocated crystals *Acta. Metall.* **1** 153–62
- Papanastasiou T C, Malamataris M and Ellwood K 1992 A new outflow boundary condition *Int. J. Numer. Methods Fluids* **14** 587–608
- Peraire J 1986 A finite element method for convection dominated flows *Ph.D. Thesis* University of Wales, Swansea
- Shu J Y, Fleck N A, Van der Giessen E and Needleman A 2001 Boundary layers in constrained plastic flow: comparison of nonlocal and discrete dislocation plasticity *J. Mech. Phys. Solids* **49** 1361–95
- Van der Giessen E and Needleman A 1995 Discrete dislocation plasticity: a simple planar model *Modelling Simul. Mater. Sci. Eng.* **3** 689–735
- Van der Giessen E and Needleman A 2003 GNDs in nonlocal plasticity theories: lessons from discrete dislocation simulations *Scr. Mater.* **48** 127–132
- Weygand D, Friedman L H, Van der Giessen E and Needleman A 2002 Aspects of boundary-value problem solutions with three-dimensional dislocation dynamics *Modelling Simul. Mater. Sci. Eng.* **10** 437–68
- Yefimov S, Groma I and Van der Giessen E 2004 A comparison of a statistical-mechanics based plasticity model with discrete dislocation plasticity calculations *J. Mech. Phys. Solids* **52** 279–300
- Zaiser M, Carmen Miguel M and Groma I 2001 Statistical dynamics of dislocation systems: the influence of dislocation–dislocation correlations *Phys. Rev. B* **64** 224102–11
- Zienkiewicz O C, Löhner R and Morgan K 1985 High speed inviscid compressive flow by the finite element method *The Mathematics of Finite Elements and Applications* vol VI (London: Academic) pp 1–25
- Zienkiewicz O C and Taylor R L 1991 *The Finite Element Method* 4th edn (New York: McGraw Hill)